


Nature of Subdiffusion Crossover in Molecular and Polymeric Glassformers

H. Srinivasan^{1,2}, V. K. Sharma^{1,2}, V. García Sakai³, and S. Mitra^{1,2}

¹*Solid State Physics Division, Bhabha Atomic Research Centre, Mumbai 400085, India*

²*Homi Bhabha National Institute, Anushaktinagar, Mumbai 400094, India*

³*ISIS Neutron and Muon Centre, Rutherford Appleton Laboratory, Didcot, United Kingdom*

 (Received 23 May 2023; revised 21 November 2023; accepted 3 January 2024; published 1 February 2024)

A crossover from a non-Gaussian to Gaussian subdiffusion has been observed ubiquitously in various polymeric and molecular glassformers. We have developed a framework that generalizes the fractional Brownian motion model to incorporate non-Gaussian features by introducing a jump kernel. We illustrate that the non-Gaussian fractional Brownian motion model accurately characterizes the subdiffusion crossover. From the solutions of the non-Gaussian fractional Brownian motion model, we gain insights into the nature of van Hove self-correlation in non-Gaussian subdiffusive regime, which is found to exhibit exponential tails, providing first such experimental evidence in molecular glassformers. The validity of the model is supported by comparison with incoherent quasielastic neutron scattering data obtained from several molecular and polymeric glassformers.

DOI: [10.1103/PhysRevLett.132.058202](https://doi.org/10.1103/PhysRevLett.132.058202)

The problem of diffusion mechanism in supercooled liquids and glasses remains an essential component in the theory of glass transitions [1–4]. The diffusion processes in these media categorically violate the basic tenets of Brownian motion such as Fickianity [linear time dependence of mean-squared displacement (MSD)] and Gaussianity (displacement distribution is Gaussian). However, such violations are often sensitive to the length and timescales explored and therefore inevitably lead to crossovers in diffusion mechanisms. These crossovers have now been experimentally observed in a wide range of systems, including colloids [5–8], molecular and ionic liquids [9,10], and polymers [4,11–13]. Colloidal suspensions exhibit a crossover from non-Fickian to Fickian regime while yet remaining non-Gaussian [5–8]. On the other hand, molecular and polymeric glassformers ubiquitously display a crossover from non-Gaussian to Gaussian diffusion while yet being non-Fickian (subdiffusive) [4,9–13]. While the latter has been observed and investigated through various simulations [4,9,14] and experiments [4,9–12,14], a first principles model has not yet been devised, which has precluded achieving a comprehensive understanding of the underlying basis for non-Gaussianity across these crossovers. Glassformers exhibit a distinct exponential decay in their displacement distribution [7,15,16], a feature observed in various complex fluids such as colloidal suspensions [5–7], Si atoms in a silica melt [16,17], and in Lennard-Jones particles [16,18]. This behavior is now understood to be a result of large deviations and randomization of number of jumps in particle displacement [19]. However, the precise nature of displacement distribution in glassformers undergoing subdiffusion crossover has not been investigated yet.

In this Letter, we develop a model for non-Gaussian fractional Brownian motion (nGfBm) and show the emergence of subdiffusion crossover through it. Further, our model also demonstrates that in the non-Gaussian subdiffusive regime, displacement distribution clearly exhibits an exponential tail. We use the nGfBm model to analyze incoherent quasielastic neutron scattering (IQENS) data of molecular and polymeric glassformers, including ethylene glycol (EG) and its deep eutectic solvents, as well as MD simulation data of pure EG. Our findings provide the first experimental evidence of exponential tails in the displacement distribution of molecular glassformers and also demonstrate the applicability of the model to other systems studied in literature [9,10].

The diffusion mechanisms and the crossovers therein can be characterized by investigating van Hove self-correlation function $G_s(r, t)$ or its time Fourier transform, self-intermediate scattering function (SISF), $I_s(Q, t)$. In glassformers the SISF is typically found to follow a stretched exponential function, $I_s(Q, t) = \exp\{-[t/\tau_s(Q)]^\beta\}$, where the stretching parameter β characterizes the deviation from an exponential relaxation profile and τ_s is the characteristic relaxation time. Various experimental [4,10,12–14] and computational [9,12,14] studies show that polymer and molecular glassformers exhibit a crossover in τ_s vs Q relationship near the first maximum, Q_0 of the structure factor. Precisely speaking, for $Q < Q_0$, $\tau(Q) \sim Q^{-2/\beta}$, while for $Q > Q_0$, $\tau(Q) \sim Q^{-2}$. At low Q values ($< Q_0$), juxtaposing the relationship $\tau_s \sim Q^{-2/\beta}$ with the stretched exponential decay, inevitably leads to a Gaussian subdiffusion with a MSD, $\langle \delta r^2(t) \rangle \sim t^\beta$. However, in the high Q regime ($> Q_0$), where $\tau_s \sim Q^{-2}$, the diffusion mechanism cannot be

described within the Gaussian approximation [4,9,13]. Therefore, this crossover in the behavior of relaxation time has been attributed to a transition from Gaussian (for $Q < Q_0$) to a non-Gaussian (for $Q > Q_0$) subdiffusion in these media [4,9,10]. In what follows, we present a characterization of the subdiffusion crossover by formulating a Fokker-Planck equation for the nGfBm model. Our results demonstrate that the emergence of the subdiffusion crossover is solely due to the nonlocality induced by jump kernel in the model.

The two salient features of glassformers are the subdiffusive behavior due to strong memory effects and non-Gaussianity arising out of large jumps. To develop a physical model to describe a crossover from non-Gaussian to Gaussian subdiffusion, it is essential to decouple these two features. Subdiffusive phenomena that originate due to a system's strong memory can be modeled using the framework of fractional Brownian motion (fBm). The standard fBm, $B_\alpha(t)$, is a self-similar centered Gaussian process with an autocorrelation $\langle B_\alpha(t_1)B_\alpha(t_2) \rangle = (t_1^\alpha + t_2^\alpha - |t_1 - t_2|^\alpha)$, where $\alpha \in (0, 2)$. We define the particle displacements in these glassy media to be driven by the standard fBm, according to $dx(t) = \sqrt{2D_\alpha}dB_\alpha(t)$, ($0 < \alpha < 1$), where D_α is the fractional diffusion constant with dimensions m^2/s^α . Using the recent developments on calculus for a fBm-driven process [20], the Fokker-Planck equation for particle displacements can be obtained to be $[\partial G_s(x, t)/\partial t] = \alpha t^{\alpha-1} D_\alpha [\partial^2 G_s(x, t)/\partial x^2]$ [21]. The solutions of this equation [29] for the initial condition, $G_s(x, 0) = \delta(x)$, yields $G_s(x, t) = (4\pi D_\alpha t^\alpha)^{-1} \exp[-x^2/(4D_\alpha t^\alpha)]$. This equation describes a Gaussian subdiffusion process where the MSD is $2D_\alpha t^\alpha$ and all the higher cumulants of displacements are zero. In order to incorporate the non-Gaussian features in the standard fBm model, we propose the following equation for non-Gaussian fBm (nGfBm):

$$\frac{\partial G_s(x, t)}{\partial t} = \alpha t^{\alpha-1} \int_{-\infty}^{\infty} dx' \Lambda(x - x') \frac{\partial^2 G_s(x', t)}{\partial x'^2}, \quad (1)$$

where $\Lambda(x - x')$ is the jump kernel that contains information about the spatially nonlocal nature of the diffusion process, allowing one to account for large amplitude jumps that are the main source of non-Gaussianity in glass dynamics [30,31]. Using $\Lambda(x) = D_\alpha \delta(x)$ allows for only local or infinitesimally small displacements and therefore reproduces the standard fBm process. The general solutions to Eq. (1) are readily obtained in the Fourier space using the SISF, $I_s(k, t) = I_0(k) \exp[-k^2 \Lambda(k) t^\alpha]$, where $\Lambda(k)$ and $I_0(k)$ are the Fourier transforms of $\Lambda(x)$ and $G_s(x, 0)$, respectively.

The general form of jump kernel in our Letter should exhibit transient non-Gaussian effects at short distances, and revert to Gaussian behavior at long distances. To be more precise, we consider a characteristic length scale for

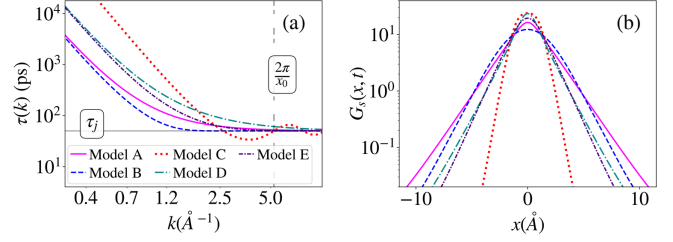


FIG. 1. (a) Variation of relaxation time with momentum transfer k for different jump-kernel models listed in Table S1 using the same set of parameters (x_0 , τ_j , α). The horizontal (solid) and vertical (dashed) lines represent values of τ_j and $2\pi/x_0$, respectively. (b) The calculated displacement distribution, $G_s(x, t)$ at $t = \tau_j$, for the case of each of these jump kernels. The final distributions are convoluted with a Gaussian ensemble for $G_s(x, 0)$.

jump processes, x_0 . The jump kernel induces non-Gaussian behavior for ($x \ll x_0$) and smoothly transitions to the Gaussian regime for ($x \gg x_0$). In the Fourier domain, these conditions can be simplified into two specific limiting rules: $\Lambda(k) \xrightarrow{kx_0 \rightarrow 0} (x_0^2/\tau_j^\alpha)$ and $\Lambda(k) \xrightarrow{kx_0 \rightarrow \infty} (k^{-2}/\tau_j^\alpha)$ [21]. Combining these rules, we propose the general jump kernel as a series expansion,

$$\Lambda(k) = \frac{k^{-2}}{\tau_j^\alpha} \sum_{n=1}^{\infty} c_n (kx_0)^{2n}, \quad (2)$$

where only the even terms are considered owing to the isotropic nature of the diffusion problem. The choice of the coefficients $\{c_n\}$ is dictated by conditions that the sum converges to unity for $kx_0 \rightarrow \infty$ and is proportional to x_0^2 for $kx_0 \rightarrow 0$. Various choices $\{c_n\}$ and their respective jump kernels are listed in Table S1 [21]. Notable choices include $(-1)^{n-1}$ and $(-1)^{n-1}/n!$, which correspond to symmetric exponential and Gaussian jump kernels that are also referred to as Model A and B in the list. Comparing the SISF of nGfBm from Eq. (1) with the $e^{-|t/\tau(k)|^\alpha}$, we get $\tau(k) \sim \tau_j [k^2 \Lambda(k)]^{-1/\alpha}$. Figure 1 shows the behavior of the dispersion relationship for five different jump kernels (Models A–E) listed in Table S1 (refer to [21]), showing a clear evidence of transition from Gaussian to non-Gaussian behavior.

The exponential nature of displacement distribution emerges from the limiting behavior $\Lambda(k) \xrightarrow{kx_0 \rightarrow \infty} (k^{-2}/\tau_j^\alpha)$. The inverse Fourier transform in this limit is $\Lambda_h(x) \sim (x_0/2\tau_j^\alpha) e^{-|x|/x_0}$. It can be explicitly shown that this limiting form of jump kernel leads to an exponential behavior in the displacement distribution [21]. The log plot of displacement distributions, $G_s(x, t)$, at $t = \tau_j$ for different models shown in Fig. 1(b) bears evidence in support of the exponential nature. In the diminishing limit of x_0 and τ_j , the jump kernel reduces to $D_\alpha \delta(x)$ (where $D_\alpha = c_1 x_0^2/\tau_j^\alpha$)

effectively restoring the Gaussian regime following fBm. Further, it is also notable that for a given set of parameters (x_0, τ_j) , the displacement distribution approaches the Gaussian limit for $t \gg \tau_j$ irrespective of the choice of jump kernel (Fig. S1).

An exact analytical solution for the symmetric exponential kernel is derived to provide insights into real-space solutions, motivated by its reliability across various systems and its emergence as a limiting distribution in highly heterogeneous scenarios. For the exponential decay kernel considered in Eq. (1) $I_s(k, t) = I_0(k) \exp\{-1/[1+(kx_0)^{-2}][t/\tau_j]^\alpha\}$. The exact solution of $I_s(k, t)$, obtained by inverting the Fourier transform [21],

$$G_s(x, t) = e^{-\hat{t}^\alpha} \left[\frac{e^{-\hat{x}}}{2x_0} \sum_{n=0}^{\infty} \frac{\hat{t}^{\alpha(n+1)}}{m_n} \hat{x}^n g_n(\hat{x}) + \delta(x) \right] \otimes G_0, \quad (3)$$

where $G_0(x)$ is the initial condition [inverse Fourier transform of $I_0(k)$] of the system and $g_n(z)$ are functions governed by a recursive relationship $g_n(z) = z^{-1}(2n-1)g_{n-1}(z) + g_{n-2}(z)$, with the first two terms being $g_0(z) = 1$ and $g_1(z) = z^{-1}(z+1)$. Here, $\hat{x} = (|x|/x_0)$ and $\hat{t} = (t/\tau_j)$ and $m_n = 2^n n!(n+1)!$. The solutions of the equation can also be given in terms of a series of modified Bessel functions, $K_n(z)$ [21]. In the strongly heterogeneous limit ($|x|/x_0 \rightarrow 0$) the solutions given in Eq. (3) shows an exponential decay in the leading term, reminiscent of the universal behavior of displacement distribution in glassforming systems [16,19], and the corrections to the exponential behavior are governed by the algebraic power series in Eq. (3). The contribution of these corrections are also related to the ratios (t/τ_j) in the series. The appearance of exponential tails is more prominent when the system is probed at times much smaller than τ_j . As the system approaches glass transition, the effective frequency of jumps decreases, leading to sharper display of exponential tails. This is consistent with the consensus that the exponential behavior of displacement distribution is enhanced near the glass transition [16]. In general, our model tends to exhibit stronger affinity to exponential tails with increasing heterogeneity (x_0 and τ_j) [21].

As observed in various other glassforming systems [4,9,10,12,13], the IQENS data of ethylene glycol (EG) and its associated deep eutectic solvents (DESS) —EG+ZnCl₂ (1:4 molar ratio) and EG + LiCl (1:3 molar ratio)—follow a stretched exponential relaxation profile based on characteristic timescale τ_s and stretching exponent β (described in SM [21]). Liquid ethylene glycol (EG) is known to exhibit stretched exponential relaxation [32,33], and it is anticipated that DESSs based on EG will also display this characteristic, given their resemblance to supercooled liquids [34]. The average relaxation time $\tau_a(Q) = \tau_s(Q)\beta^{-1}\Gamma(\beta^{-1})$ is calculated from IQENS data fitting. Figure S4 clearly indicates the crossover from Gaussian dynamics at low Q to non-Gaussian behavior at higher Q values for EG and the DESSs.

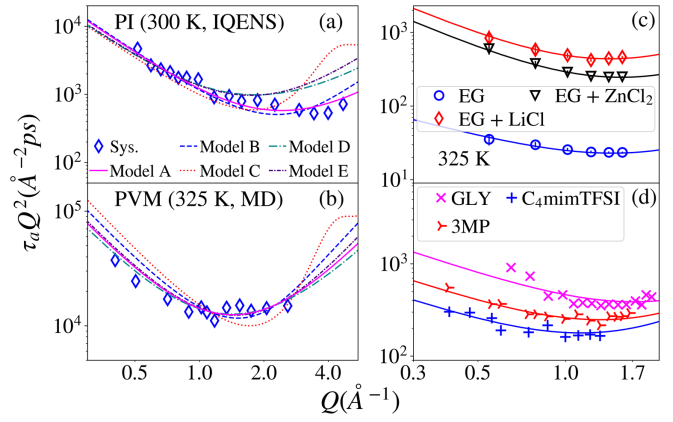


FIG. 2. (a) Plot of $\tau_a Q^2$ vs Q for (a) polyisoprene (PI) [4] and (b) polyvinyl methyl ether (PVM) [12] with fits based on five different jump kernels (Models A–E). The exponential kernel (Model A) suits the best over a wide Q range and hence employed in modeling systems with limited Q range. Plot of $\tau_a Q^2$ vs Q for (c) EG, EG + LiCl, and EG + ZnCl₂ at 325 K and (d) different systems from literature (GLY, glycerol [9]; 3MP, 3-methylpentane [10]; C₄mimTFSI, 1-butyl-3-methylimidazolium bis(trifluoromethanesulfonyl)imide [10]) along with fits based on Model A.

Figures 2(a) and 2(b) show the variation of relaxation time τ_a in polymeric systems, as observed from IQENS experiments for polyisoprene (PI) [4] and MD simulations of polyvinyl methylether (PVM) [12]. Similar plots for the systems investigated in this Letter (EG and their DESSs) and other molecular organic glassformers [9,10] are also shown in Figs. 2(c) and 2(d), respectively. As illustrated in the plots, these systems show a crossover from $Q^{-2/\beta}$ (for $Q < 1 \text{ \AA}^{-1}$) to Q^{-2} (for $Q > 1 \text{ \AA}^{-1}$).

To model the observed crossover in the experimental IQENS studies, we extend the nGfBm [Eq. (1)] to 3D systems using a three-dimensional fBm process with an autocorrelation of the form $\langle \mathbf{r}(t_1) \cdot \mathbf{r}(t_2) \rangle = 3D_\alpha (t_1^\alpha + t_2^\alpha - |t_1 - t_2|^\alpha)$. It has been shown that an n -dimensional fBm process can be constructed as a linear superposition of n independent fBm processes [35]. This allows us to construct an extension of Eq. (1) for the 3D nGfBm [21]. The 3D jump kernels can also be chosen based on the Eq. (2) with parameters r_0 and τ_j subject to an additional constraint of radial symmetry. The Q dependence of the average relaxation time follow $\tau_a(Q) = [Q^2 \Lambda(Q)]^{-1/\alpha}$, which we use to fit the Q dependence of the measured τ_a for all the systems using models based on different jump kernels listed in Table S1 [21].

For PI and PVM, Figs. 2(a) and 2(b) demonstrate that model A (exponential jump kernel) provides the fits in the extended Q range. Figures 2(c) and 2(d) showcase the versatility of the exponential kernel [36] across a diverse range of systems, including EG, EG-based DESSs, glycerol (GLY), 3-methylpentane (3MP), and the ionic liquid C₄mimTFSI. This highlights the robustness of the

nGfBm model, which works for IQENS measurements carried out using different spectrometers with varying resolutions and in particular also emphasizes the larger applicability of exponential kernel.

Evidently, the model represents the data very well and captures the crossover from Gaussian dynamics at low Q to non-Gaussian behavior at higher Q values for all the systems. The model parameters r_0 and τ_j provide valuable insights into the extent of dynamical heterogeneity in the system. For the specific case of the exponential kernel, the crossover point in Q space is linked to r_0 and can be precisely estimated as $Q^* = \sqrt{(1/\beta) - 1}/r_0$ ($\beta \neq 1$). This implies that crossover point is inversely related to the extent of spatial heterogeneity in the nonlocal diffusive process. As $r_0 \rightarrow 0$, representing a completely homogeneous limit, Q^* tends to infinity, resulting in Gaussian subdiffusion regime at all length scales. The values of Q^* for different glassforming systems with varying fragility index are listed in Table S3 in the SM [21]. The ability to model self-diffusion in wide range of systems with different fragility indices indicates the robustness of the nGfBm model. Notably, r_0 shows minimal temperature variation, suggesting that the crossover point Q^* is largely unaffected by temperature changes. Meanwhile, the jump time, τ_j , shows a remarkable increase with decrease in temperature, as glass transition is approached. It is notable that the increase in the jump times τ_j essentially dictates that the non-Gaussianity in the diffusion process is enhanced as the system approaches glass transition. We also find that Q^* typically lies in the 1–2 \AA^{-1} (Table S4) [31] for all the glassformers that have been investigated so far. These results, while consistent with the existing literature, reinforces the idea that the origin of subdiffusion crossover is linked to the length scale of nonlocal jumps in the diffusion process

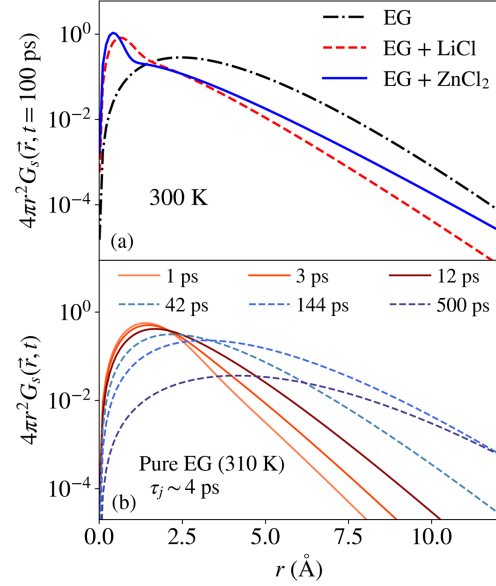


FIG. 3. (a) The radial van Hove self-correlation function calculated from Eq. (4) based on the parameters $(\tau_j, \beta, r_0, \langle u^2 \rangle)$ extracted from experimental IQENS fits for pure EG and DESs (EG + LiCl, EG + ZnCl₂) at $T = 300$ K and $t = 100$ ps. (b) Radial van Hove self-correlation function for pure EG (310 K) calculated at different times t ; $t > 10\tau_j$ are shown by broken lines and $t < 10\tau_j$ are shown by solid lines.

rather than its relationship with the first maxima of the structure factor peak.

In order to shed more light on the transition from non-Gaussian to Gaussian behavior, we calculate the 3D van Hove self-correlation function from the model. Focusing on radially symmetric kernel, we have $I(Q, t) = \exp[-(Qr_0)^2 / (1 + (Qr_0)^2)(t/\tau_j)^\beta]$. Using this, the van Hove self-correlation function in this case is

$$G_s(\mathbf{r}, t) = e^{-(t/\tau_j)^\beta} \left[\frac{1}{8\pi r_0^3} e^{-(r/r_0)} \sum_{n=0}^{\infty} \frac{(t/\tau_j)^{\beta(n+1)}}{(n+1)!n!} \left(\frac{r}{2r_0}\right)^{n-1} g_{n-1}\left(\frac{r}{r_0}\right) + \delta(\mathbf{r}) \right] \otimes \left(\frac{3}{4\pi\langle u^2 \rangle}\right)^{3/2} e^{-3r^2/(4\langle u^2 \rangle)}. \quad (4)$$

The first term in Eq. (4) describes the heterogeneous diffusion process with a typical exponential displacement distribution in the leading order, while the second term represents the Gaussian thermal cloud generated by fast localized dynamics. For $t \ll \tau_j$, the radial van Hove self-correlation function $[4\pi r^2 G_s(\mathbf{r}, t)]$ is typically a sum of Gaussian thermal cloud near origin with exponential tails at large values of r . As time progresses, the contribution of the diffusive component becomes dominant and the second term decreases at a rate governed by $e^{-(t/\tau_j)^\beta}$. Figure 3(a) shows the plots of $4\pi r^2 G_s(\mathbf{r}, t = 100 \text{ ps})$ for the DESs and pure EG, directly computed with set of parameters $(r_0, \tau_j, \alpha, \langle u^2 \rangle)$ obtained from the fits of the QENS spectra

at 300 K. The significantly different values of τ_j for EG and DESs, being 7 ps and 200 ps, respectively, account for the marked disparity in their curves. In DESs, longer τ_j causes the initial peaks ($r < 2 \text{ \AA}$) in van Hove self-correlation function to be more pronounced. These peaks have vanished in the case of pure EG, as the fast local dynamics have completely relaxed and the dynamics is described as a purely diffusive process at 100 ps. Further, the tails prominently exhibit an exponential decay in the cases of both the DESs but shows a nearly Gaussian behavior for pure EG. A clearer perspective of these changes is apparent from the plots of radial van Hove self-correlation of pure EG (310 K) at different times (ranging from 1 to 500 ps) in

Fig. 3(b). Typically, it is observed that the exponential tails are discernible for $t < 10\tau_j$. The curves for $t < 10\tau_j$ and $t > 10\tau_j$ are marked by solid and broken lines, respectively, to clearly indicate this feature and exhibit the crossover from non-Gaussian to Gaussian regime.

In order to check the veracity of the model, we have calculated the radial van Hove self-correlation function from MD simulations of pure EG and tried to fit it with Eq. (4). The parameters from the fit were optimized so as to describe the simulated data over a reasonable time window (0–500 ps). In order to achieve a consistent model, the fitting was carried out at different times and model parameters were optimized across all the times. The extracted parameters are found to be fairly consistent with experimental observations. The simulated van Hove self-correlation function and their respective fits are given in Fig. S8.

The diffusion landscape in glassformers exhibits various crossovers entailing different mechanisms. Universally, molecular and polymeric glassformers exhibit an inherent crossover from non-Gaussian to Gaussian subdiffusion. In this Letter, we have characterized the nature of particle displacements across this crossover by augmenting the framework of fBm to incorporate nonlocal jumps. The constructed model provides a generalized mathematical structure that can be used to describe a number of such processes that simultaneously involve both non-Markovianity and spatial jumps in a diffusion process. We present a generalized jump kernel that elucidates the subdiffusion crossover, revealing the emergence of an exponential kernel as a consequence of physical constraints. The case of exponentially distributed jumps is solved providing a link between the crossover point and the extent of heterogeneity in the system. Notably, this framework also highlights the exponential nature of van Hove self-correlation function during the non-Gaussian subdiffusion regime.

-
- [1] W. Gotze and L. Sjogren, Relaxation processes in supercooled liquids, *Rep. Prog. Phys.* **55**, 241 (1992).
- [2] W. Kob, C. Donati, S. J. Plimpton, P. H. Poole, and S. C. Glotzer, Dynamical heterogeneities in a supercooled Lennard-Jones liquid, *Phys. Rev. Lett.* **79**, 2827 (1997).
- [3] P. G. Debenedetti and F. H. Stillinger, Supercooled liquids and the glass transition, *Nature (London)* **410**, 259 (2001).
- [4] A. Arbe, J. Colmenero, F. Alvarez, M. Monkenbusch, D. Richter, B. Farago, and B. Frick, Non-Gaussian nature of the α relaxation of glass-forming polyisoprene, *Phys. Rev. Lett.* **89**, 245701 (2002).
- [5] R. Pastore, A. Ciarlo, G. Pesce, F. Greco, and A. Sasso, Rapid Fickian yet non-Gaussian diffusion after subdiffusion, *Phys. Rev. Lett.* **126**, 158003 (2021).
- [6] F. Rusciano, R. Pastore, and F. Greco, Fickian non-Gaussian diffusion in glass-forming liquids, *Phys. Rev. Lett.* **128**, 168001 (2022).
- [7] B. Wang, S. M. Anthony, S. C. Bae, and S. Granick, Anomalous yet Brownian, *Proc. Natl. Acad. Sci. U.S.A.* **106**, 15160 (2009).
- [8] B. Wang, J. Kuo, S. C. Bae, and S. Granick, When Brownian diffusion is not Gaussian, *Nat. Mater.* **11**, 481 (2012).
- [9] R. Busselez, R. Lefort, A. Ghoufi, B. Beuneu, B. Frick, F. Affouard, and D. Morineau, The non-Gaussian dynamics of glycerol, *J. Phys. Condens. Matter* **23**, 505102 (2011).
- [10] M. Kofu, A. Faraone, M. Tyagi, M. Nagao, and O. Yamamuro, Two inherent crossovers of the diffusion process in glass-forming liquids, *Phys. Rev. E* **98**, 042601 (2018).
- [11] A. Arbe, J. Colmenero, F. Alvarez, M. Monkenbusch, D. Richter, B. Farago, and B. Frick, Experimental evidence by neutron scattering of a crossover from Gaussian to non-Gaussian behavior in the α relaxation of polyisoprene, *Phys. Rev. E* **67**, 051802 (2003).
- [12] S. Capponi, A. Arbe, F. Alvarez, J. Colmenero, B. Frick, and J. P. Embs, Atomic motions in poly(vinyl methyl ether): A combined study by quasielastic neutron scattering and molecular dynamics simulations in the light of the mode coupling theory, *J. Chem. Phys.* **131**, 204901 (2009).
- [13] A. Arbe, J. Colmenero, M. Monkenbusch, and D. Richter, Dynamics of glass-forming polymers: “Homogeneous” versus “heterogeneous” scenario, *Phys. Rev. Lett.* **81**, 590 (1998).
- [14] J. Colmenero, F. Alvarez, and A. Arbe, Self-motion and the α relaxation in a simulated glass-forming polymer: Crossover from Gaussian to non-Gaussian dynamic behavior, *Phys. Rev. E* **65**, 041804 (2002).
- [15] M. V. Chubynsky and G. W. Slater, Diffusing diffusivity: A model for anomalous, yet Brownian, diffusion, *Phys. Rev. Lett.* **113**, 098302 (2014).
- [16] P. Chaudhuri, L. Berthier, and W. Kob, Universal nature of particle displacements close to glass and jamming transitions, *Phys. Rev. Lett.* **99**, 060604 (2007).
- [17] L. Berthier, G. Biroli, J. P. Bouchaud, W. Kob, K. Miyazaki, and D. R. Reichman, Spontaneous and induced dynamic correlations in glass formers. II. Model calculations and comparison to numerical simulations, *J. Chem. Phys.* **126**, 184504 (2007).
- [18] L. Berthier and W. Kob, The Monte Carlo dynamics of a binary Lennard-Jones glass-forming mixture, *J. Phys. Condens. Matter* **19**, 205130 (2007).
- [19] E. Barkai and S. Burov, Packets of diffusing particles exhibit universal exponential tails, *Phys. Rev. Lett.* **124**, 060603 (2020).
- [20] T. E. Duncan, Y. Hu, and B. Pasik-Duncan, Stochastic calculus for fractional Brownian motion I. Theory, *SIAM J. Control Optim.* **38**, 582 (2000).
- [21] See Supplemental Material at <http://link.aps.org/supplemental/10.1103/PhysRevLett.132.058202> for detailed mathematical derivations and more information about experiments and simulations, which includes Refs. [22–28].
- [22] B. B. Mandelbrot and J. W. Van Ness, Fractional Brownian motions, fractional noises and applications, *SIAM Rev.* **10**, 422 (1968).
- [23] C. J. Carlile and M. A. Adams, The design of the iris inelastic neutron spectrometer and improvements to its analysers, *Physica (Amsterdam)* **182B**, 431 (1992).

- [24] P. Kumar, S. R. Varanasi, and S. Yashonath, Relation between the diffusivity, viscosity, and ionic radius of LiCl in water, methanol, and ethylene glycol: A molecular dynamics simulation, *J. Phys. Chem. B* **117**, 8196 (2013).
- [25] G. Gygli, X. Xu, and J. Pleiss, Meta-analysis of viscosity of aqueous deep eutectic solvents and their components, *Sci. Rep.* **10**, 21395 (2020).
- [26] A. P. Abbott, J. C. Barron, K. S. Ryder, and D. Wilson, Eutectic-based ionic liquids with metal-containing anions and cations, *Chem. Eur. J.* **13**, 6495 (2007).
- [27] J. C. Phillips, R. Braun, W. Wang, J. Gumbart, E. Tajkhorshid, E. Villa, C. Chipot, R. D. Skeel, L. Kalé, and K. Schulten, Scalable molecular dynamics with NAMD, *J. Comput. Chem.* **26**, 1781 (2005).
- [28] R. B. Best, X. Zhu, J. Shim, P. E. M. Lopes, J. Mittal, M. Feig, and A. D. MacKerell, Optimization of the additive charmm all-atom protein force field targeting improved sampling of the backbone ϕ , ψ and side-chain χ_1 and χ_2 dihedral angles, *J. Chem. Theory Comput.* **8**, 3257 (2012).
- [29] W. Wang, R. Metzler, and A. G. Cherstvy, Anomalous diffusion, aging, and nonergodicity of scaled Brownian motion with fractional Gaussian noise: Overview of related experimental observations and models, *Phys. Chem. Chem. Phys.* **24**, 18482 (2022).
- [30] M. Bier, R. van Roij, M. Dijkstra, and P. van der Schoot, Self-diffusion of particles in complex fluids: Temporary cages and permanent barriers, *Phys. Rev. Lett.* **101**, 215901 (2008).
- [31] B. Vorselaars, A. V. Lyulin, K. Karatasos, and M. A. J. Michels, Non-Gaussian nature of glassy dynamics by cage to cage motion, *Phys. Rev. E* **75**, 011504 (2007).
- [32] V. Crupi, D. Majolino, P. Migliardo, and V. Venuti, Diffusive relaxation processes and low-frequency dynamical properties in bulk and confined ethylene glycol by neutron spectroscopy, *J. Chem. Phys.* **118**, 5971 (2003).
- [33] O. Sobolev, A. Novikov, and J. Pieper, Quasielastic neutron scattering and microscopic dynamics of liquid ethylene glycol, *Chem. Phys.* **334**, 36 (2007).
- [34] S. Banerjee, P. K. Ghorai, S. Das, J. Rajbangshi, and R. Biswas, Heterogeneous dynamics, correlated time and length scales in ionic deep eutectics: Anion and temperature dependence, *J. Chem. Phys.* **153**, 234502 (2020).
- [35] J.-H. Jeon and R. Metzler, Fractional Brownian motion and motion governed by the fractional Langevin equation in confined geometries, *Phys. Rev. E* **81**, 021103 (2010).
- [36] The fits based on different models (Models A–E) are explicitly shown in Fig. S4 in the Supplemental Material. Within the limited Q range in the case of IQENS measurements on molecular systems different models arising from different jump kernels exhibit a very similar behavior.